11th International Symposium on Turbulence and Shear Flow Phenomena (TSFP11)
Southampton, UK, July 30 to August 2, 2019

SCALAR DISPERSION IN A MULTI-SCALE GENERATED TURBULENT FLOW

Oliver R. H. Buxton
Department of Aeronautics
Imperial College London
UK
o.buxton@imperial.ac.uk

Paweł Baj
Department of Energy and Process Engineering
NTNU
Norway
pawel.baj@ntnu.no

ABSTRACT

Combined PLIF and PIV experiments were performed in the near-wake region of a multi-scale array of three different length scales. We document, and measured terms of the multi-scale triple-decomposed energy budget and show the importance of non-linear interactions between the primary shedding structures in multi-scale generated turbulence. We subsequently observe a cascade of scalar bursting events, in which the scalar is transported a large distance in the transverse direction over a short period of time. These bursts unfolded spatially, such that they were observed between the small and medium wakes and the medium and large wakes. These bursts were also observed in the wake of a single-scale array of objects of comparable blockage to the multi-sale array, but there was no cascade of bursts identified and they all occurred in the same spatial location. Combined, these findings verify the space-scale unfolding (SSU) mechanism originally postulated in Laizet & Vassilicos (2012). By performing the multi-scale triple decomposition of Baj *et al.* (2015) we show that the dominant mode in the scalar transport is that associated to the fundamental shedding of the larger of the two intersecting wakes. We thus conclude that the SSU mechanism is subtly different to that originally postulated by Laizet & Vassilicos (2012). Those authors originally attributed the SSU mechanism to the coherence of the overall, Reynolds-decomposed velocity fluctuation u'. Here we show that the dominant effect is in fact the coherent part of the fluctuating velocity concordant with the fundamental shedding frequency of the larger of the two interacting wakes. Downstream of the wake intersection point this particular coherent scalar flux component is the major contributor to the overall scalar flux.

INTRODUCTION

Many turbulent flows are triggered by the instability of large-scale coherent motions embedded within the flow, such as the von Kármán vortex street of a cylinder wake. Given the high energy content within these coherent motions Hussain & Reynolds (1970) proposed a triple decomposition of the velocity field in which the classical Reynolds-decomposed fluctuating velocity is further decomposed into a coherent and stochastic part, $u = \overline{u} + u' = \overline{u} + \tilde{u} + u''$. In many cases, however, turbulence is triggered at a number of length scales simultaneously (e.g. flows through a forest or a cityscape). It is reasonable to expect that at each of these levels some sort of flow regularisation is enforced, resulting in coherence being introduced into the flow on top of the stochastic turbulent motion. In this regard, features of single- and multi-scale generated turbulence can diverge as the former lacks the dynamical interplay of the embedded multi-scale coherent motions. Indeed, recently, multi-scale generated turbulence has been shown to have some beneficial properties in terms of mixing performance relative to turbulence generated by a single length scale only (Goh *et al.*, 2013; Cafiero *et al.*, 2014; Laizet & Vassilicos, 2015). Since coherence is introduced at multiple length scales (and hence frequencies) simultaneously in multi-scale generated turbulence the single-scale triple decomposition of Hussain & Reynolds (1970) is insufficient to describe the dynamical interplay between these scales. For this reason Baj *et al.* (2015) developed a multi-scale triple decomposition, based on the optimal mode decomposition (Wynn *et al.*, 2013), where the velocity is decomposed as

$$u(x,t) = \overline{u}(x) + \sum_l \tilde{u}^l(x,t) + u''(x,t) \tag{1}$$

in which there are a number of coherent motions $\tilde{u}^l$ with corresponding phase signals $\phi^l(t)$. Note that the coherent modes $\tilde{u}^l$ have a temporal dependence on both the phase signal $\phi^l(t)$ as well as a slowly varying amplitude signal $A(t)$; see Baj & Buxton (2017) for more details.

We now extend this analysis to examine the dispersion of passive scalar in a multi-scale generated flow. Laizet & Vassilicos (2012) postulated the existence of the "space-scale unfolding" (SSU) mechanism, in which the spatial unfolding of the various sized wakes of a multi-scale array leads to an enhancement of the scalar transport and stirring

relative to a single-scale array. We shall trace the exchange of passive scalar between intersecting wakes in order to verify the SSU mechanism and seek its physical origins.

METHODOLOGY

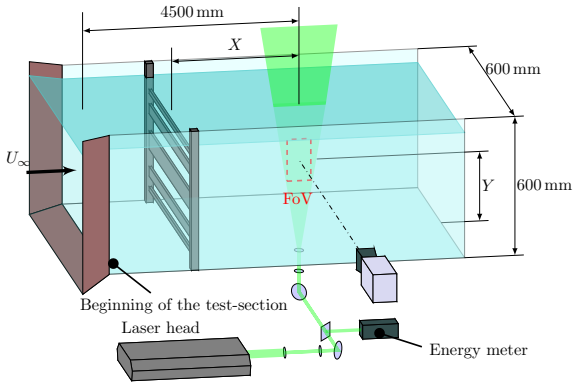

Figure 1: Experimental setup.

In this work we consider a "canonical" multi-scale flow: a symmetrical (about the centre-line), two-dimensional array (size $H \times H$) of bars with three different widths, the largest of which is positioned in the centre and the smallest at the peripheries as illustrated in fig. 1. Passive scalar (an aqueous solution of rhodamine 6G) was introduced isokinetically into the wake of the smallest bar via a micro-dosing pump in order to mimic the originally postulated SSU mechanism described in Laizet & Vassilicos (2012). Simultaneous time-resolved PIV and PLIF measurements were performed in the near-wake region of the multi-scale array. The PLIF images were converted into scalar concentration using the calibration method of Baj *et al.* (2016) which accounts for non-linear effects such as high scalar concentration and secondary fluorescence. Accounting for these effects is shown to be crucial in matching the scalar mass flux calculated from the PLIF measurements to that measured by the dye-seeding pump. Full details of the PIV and PLIF experiments, and the quantification of the scalar concentration from the PLIF images can be found in Baj & Buxton (2019).

Figure 2 illustrates the mean streamwise velocity and r.m.s. of the fluctuating velocity field (from the classical Reynolds decomposition) and the spatial organisation of the various bars. The wake intersection points, defined as saddle points in the r.m.s. field, are denoted with black crosses.

RESULTS AND DISCUSSION

Coherent Velocity Modes and Inter-scale Energy Transfer

First we consider the compensated power spectral densities (PSDs) of the transverse velocity fluctuations in the near-wake region downstream of the multi-scale array. Figure 3 shows these compensated PSDs at four particular spatial locations. These range from immediately downstream of the array at $x/H = 0.07$ (a), the intersection point between the small and medium wakes at $x/H = 0.24$ (b), the

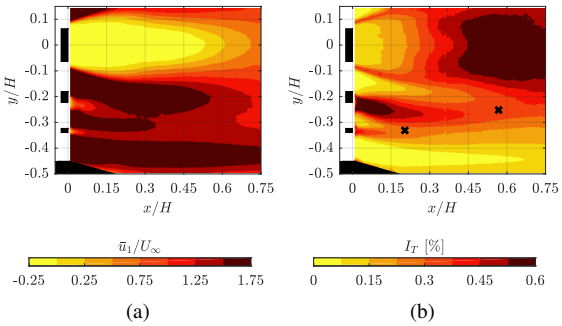

Figure 2: (a) Mean streamwise velocity field and (b) turbulence intensity field in the near-wake region. The wake intersection points are denoted with a cross on the turbulence intensity field.

intersection point between the large and the medium wake at $x/H = 0.57$ (d) and a point between the two wake intersection points at $x/H = 0.41$ (c). This spectral analysis shows that immediately downstream of the bars energetic peaks can be observed at the fundamental shedding frequencies of the three different sized bars, denoted f^I (the lowest frequency, produced by the largest bar), f^{II} and f^{III} (the highest frequency, produced by the smallest bar). However, at the location at which the smallest and medium wakes intersect additional peaks are observed in the spectra at frequencies $f^{III} \pm f^{II}$, denoted with green arrows in fig. 3(b). These peaks are also localised in space, such that the higher frequency of these secondary peaks appears only within the shear layer between the two wakes, whereas the lower frequency of the two secondary peaks appears in the opposite shear layer of the small wake. Note that the low frequency secondary peak is more persistent spatially than both the high frequency secondary peak and the higher frequency of the primary (shedding) peaks in fig. 3(c) and (d).

Precisely the same qualitative picture is observed at the second wake intersection point at $x/H = 0.57$, i.e. that between the large and the medium wakes, in fig. 3(d). Here again a high frequency secondary peak is observed in the shear layer between the two interacting wakes and a low frequency secondary peak is observed in the opposite shear layer of the smaller of the two interacting wakes. At both wake intersection points the secondary spectral peaks appear at precisely defined frequencies of $f^{III} \pm f^{II}$ at the first wake intersection point ($x/H = 0.24$) and $f^{II} \pm f^{I}$ at the second wake intersection point ($x/H = 0.57$). These spectral peaks are thus attributed to the formation of secondary coherent structures through triadic non-linear interactions between the primary coherent (shedding) modes.

By using the multi-scale triple decomposition first described in Baj *et al.* (2015), and refined in Baj & Buxton (2017), it is possible to decompose the flow field according to eq. (1). In particular it is possible to extract coherent velocity fluctuations corresponding to all of the spectral peaks identified in fig. 3, i.e. $\tilde{u}^I, \tilde{u}^{II-I}, \tilde{u}^{II}, \tilde{u}^{II+I}, \tilde{u}^{III-II}, \tilde{u}^{III}, \tilde{u}^{III+II}$ corresponding to frequencies f^I, f^{II-I} etc. By then taking the dot product of particular velocity components, i.e. the mean, coherent or stochastic fluctuations, with the Navier-Stokes equations - triple-decomposed in the multi-scale fashion described in eq. (1) - Baj & Buxton (2017) derived the multi-scale triple-decomposed energy budgets for the first time. Here we shall focus on the energy budget for the l^{th}coherent velocity fluc-

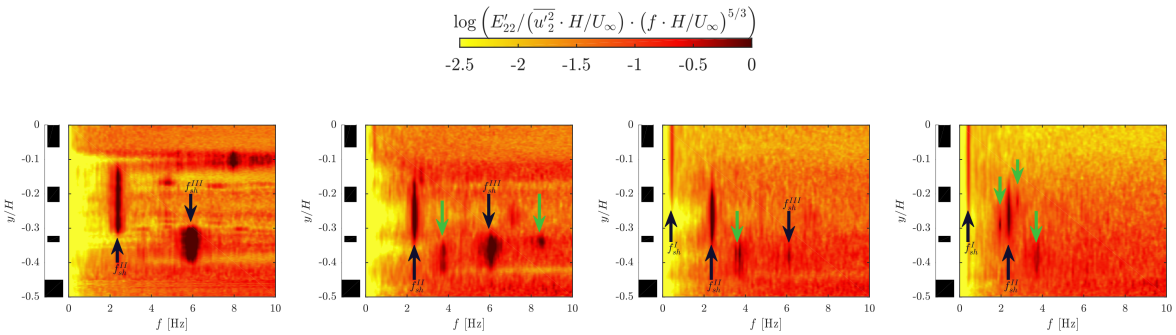

Figure 3: Compensated PSDs of the transverse velocity fluctuations at $x/H =$ (a) 0.07, (b) 0.24, (c) 0.41 and (d) 0.57.

tuations, which symbolically can be written as

$$\tilde{\mathscr{L}}^l + \tilde{\mathscr{C}}^l = \tilde{\mathscr{P}}^l - \hat{\mathscr{P}}^l + \tilde{\mathscr{T}}^l_+ - \tilde{\mathscr{T}}^l_- - \tilde{\varepsilon}^l + \tilde{\mathscr{D}}^l. \quad (2)$$

Here there are some standard looking terms, familiar from the single-scale triple decomposed energy budgets of Hussain & Reynolds (1970). These are an unsteady term $\tilde{\mathscr{L}}^l$, a convective term $\tilde{\mathscr{C}}^l$, a production term in which energy is transferred from the mean flow into the l^{th}coherent mode $\tilde{\mathscr{P}}^l$, a production term for stochastic turbulent kinetic energy directly from the l^{th}coherent mode $\hat{\mathscr{P}}^l$, a dissipation term directly from the l^{th}coherent mode $\tilde{\varepsilon}^l$ and a diffusive energy transfer $\tilde{\mathscr{D}}^l$. However, our multi-scale triple decomposed energy budgets yielded two new terms, defined as

$$\tilde{\mathscr{T}}^l_+ = -\frac{1}{2}\sum_{m,n}\overline{\tilde{u}^l_i\tilde{u}^m_j\frac{\partial\tilde{u}^n_i}{\partial x_j}} \quad (3)$$

$$\tilde{\mathscr{T}}^l_- = -\frac{1}{2}\sum_{m,n}\overline{\tilde{u}^n_i\tilde{u}^m_j\frac{\partial\tilde{u}^l_i}{\partial x_j}}. \quad (4)$$

We may thus interpret $\tilde{\mathscr{T}}^l_+$ as a source of energy into coherent mode l, draining energy from coherent mode n and $\tilde{\mathscr{T}}^l_-$ as a sink of energy from coherent mode l into coherent mode n. In both cases coherent mode m acts as a catalyst to this energy transfer. We thus combine these two terms and refer to $(\tilde{\mathscr{T}}^l_+ - \tilde{\mathscr{T}}^l_-)$ as the triadic production term, i.e. the net transfer of energy into/out of the l^{th} coherent mode through non-linear triadic interactions between coherent velocity fluctuations.

Figure 4 shows the transverse profiles of this triadic production term at the wake intersection point between the small and medium wakes at $x/H = 0.24$. Qualitatively similar behaviour is also observed at the second wake intersection point between the large and medium wakes at $x/H = 0.57$ but this is not shown for brevity. Figure 4(c) presents the integral of these transverse profiles and thus reveals the flow physics leading to the formation of the secondary coherent structures. It can be seen that the high frequency primary coherent mode $\tilde{u}^{III}$ gives up a roughly equal portion of its energy to both secondary coherent modes. However, the high frequency secondary coherent structure then transfers its energy to the low frequency primary (shedding) coherent mode which then passes this energy on to the low frequency secondary coherent mode. Again, qualitatively similar behaviour is observed at the second wake

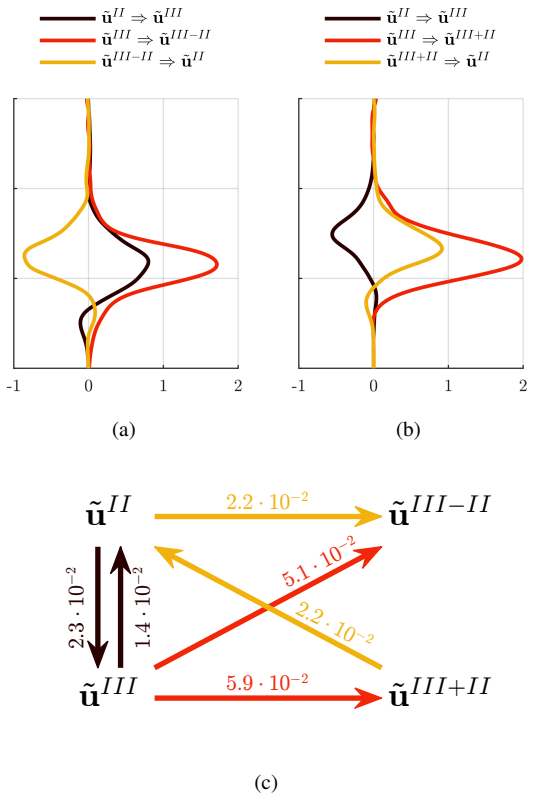

Figure 4: Components of the triadic production term of the coherent energy budget governing the transfer of energy between the primary and secondary coherent structures at the wake intersection point between the small and medium wakes for the triads (a) $\{\tilde{u}^{II}, \tilde{u}^{III}, \tilde{u}^{III-II}\}$ and (b) $\{\tilde{u}^{II}, \tilde{u}^{III}, \tilde{u}^{III+II}\}$. (c) Integral of the transverse profiles of the triadic production term's components.

intersection point between the large and medium wakes at $x/H = 0.57$ but this is not shown for brevity. This picture is also consistent with the observation that the low frequency secondary coherent mode is more persistent spatially than the high frequency primary coherent mode in fig. 3(c) and (d). We thus observe an inverse cascade in which energy is transferred from a high frequency primary coherent structure to a lower frequency secondary coherent structure un-

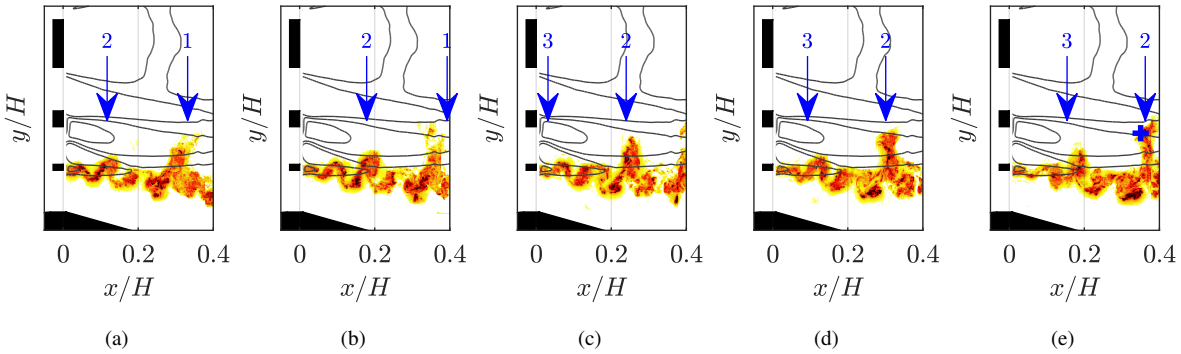

Figure 5: Consecutive qualitative PLIF images (arbitrary scale) captured downstream of the multi-scale array. The blue arrows indicate the positions of transverse scalar bursts.

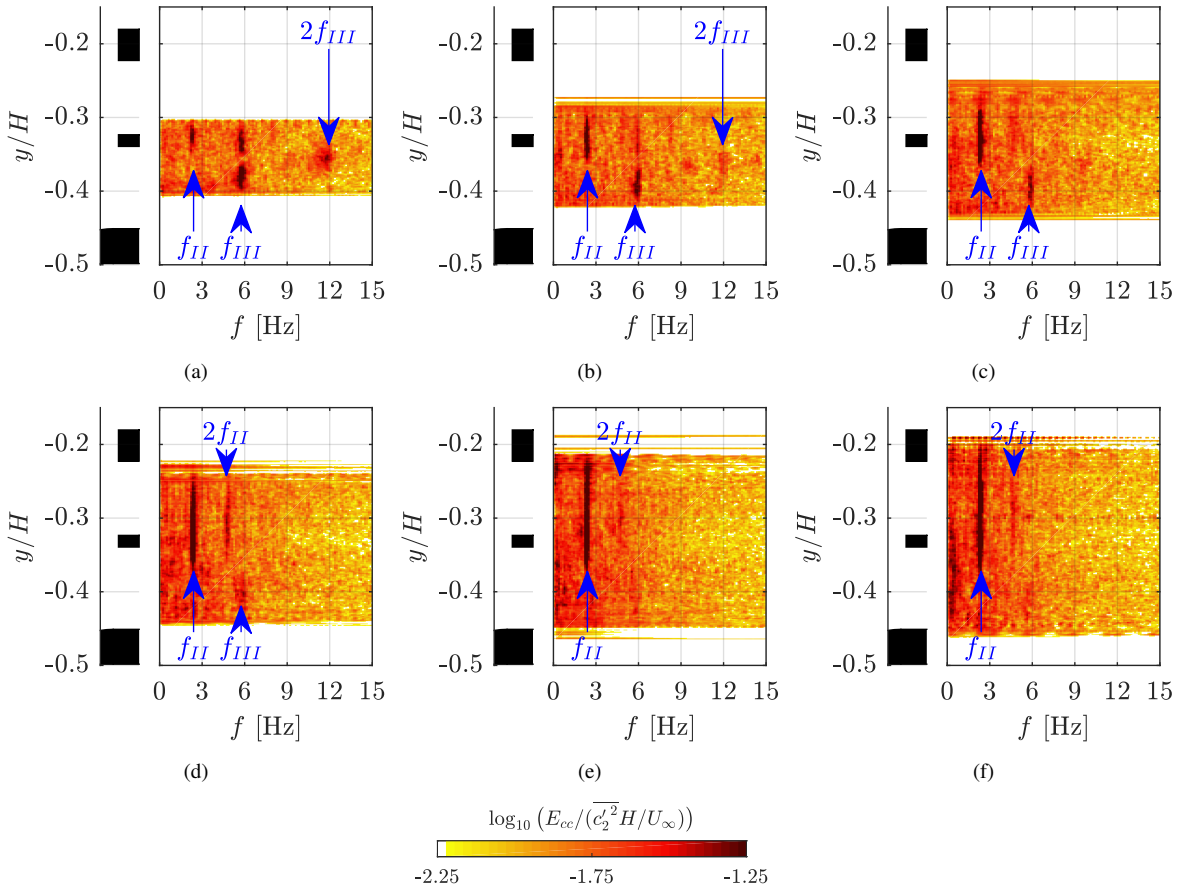

Figure 6: Power spectral densities of the scalar concentration fluctuations evaluated at: (a) $x/H = 0.12$, (b) $x/H = 0.18$, (c) $x/H = 0.24$, (d) $x/H = 0.30$, (e) $x/H = 0.36$ and (f) $x/H = 0.42$.

der the catalytic action of a lower frequency primary coherent mode.

By observing the spatial variation in the locations of the wake intersection points, and observing at least qualitatively similar flow physics at both wake intersection points, we are hinting at a manifestation of the postulated SSU mechanism. We will now verify this by observing the scalar exchange between the various wakes and try to link this scalar exchange to the multi-scale flow physics that we summarise above. A full exposition of these multi-scale energy transfers can be found in Baj & Buxton (2017).

Coherent Concentration Modes and Verification of the SSU Mechanism

Figure 5 shows an example of the "scalar bursting" phenomenon, in which a large transverse excursion of the scalar is seen from the small wake. This phenomenon was observed regularly in the multi-scale array described in the current work but only intermittently in a single-scale array of comparable blockage that was also tested. Note that this burst occurs at the location of the wake intersection point between the medium and large wakes. We thus physically verify the SSU mechanism.

Figure 6(a) to fig. 6(f) show the spatial evolution of the

PSD of the concentration fluctuations from $x/H = 0.12$ to $x/H = 0.42$. Recall that the first wake intersection point is at $x/H = 0.24$. Figure 6(a) and fig. 6(b) are thus upstream of this intersection point, fig. 6(c) is at the intersection point and fig. 6(d)-(f) are downstream of this point. In the PSDs upstream of the wake intersection point there is a strong signal at a frequency of f^{III} (the fundamental shedding mode in the wake of the smallest bar into which the scalar was seeded) which is initially partitioned between the "inner" shear layer between the wakes of the small and medium bars and the "outer" shear layer below the small wake. The second harmonic is also visible. The "inner" peak, however, is not spatially persistent and has all but disappeared by the second interrogation region in fig. 6(b). Instead, there is a dominant peak at frequency f^{II}, which corresponds to the fundamental shedding frequency of the medium wake in positions upstream of the wake intersection points, despite the scalar being seeded into the wake of the small bar. This spectral peak becomes increasingly dominant with downstream distance, with the second harmonic becoming visible in fig. 6(d)-(f). Of significance, however, is the absence of any peaks at frequencies $f^{III} \pm f^{II}$. These were identified as being caused by secondary coherent structures formed from the triadic interaction of the primary (shedding) coherent structures. This absence suggests that the secondary coherent structures do not play a major role in the transport of scalar in multi-scale generated turbulence.

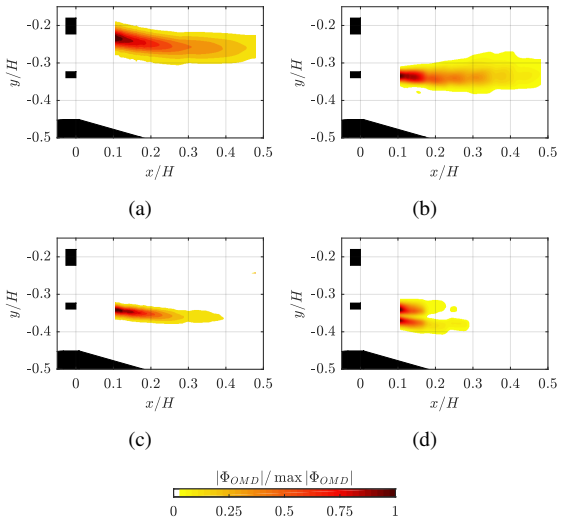

Figure 7: Energies of the normalised coherent velocity modes associated with frequencies (a) f^{II} and (c) f^{III} in addition to the variance of the normalised coherent mode for scalar concentration associated with frequency (b) f^{II} and (d) f^{III}.

We now perform the triple decomposition of eq. (1) on the fluctuations of scalar concentration to yield the coherent concentration modes. The methodology to compute the coherent velocity modes is fully described in Baj & Buxton (2017) and that to compute the coherent concentration modes is fully described in Baj & Buxton (2019). In both cases the methodologies are based on the method proposed in Baj *et al.* (2015). Given that peaks in the concentration spectra are only observed at frequencies f^{II} and f^{III}, the primary shedding frequencies of the medium and small bars respectively, only the coherent velocity and concentration modes at these frequencies are presented. Note that whilst there is a significant energy content in the coherent velocity modes affiliated with frequencies $f^{III} \pm f^{II}$ there is negligible concentration variance in such coherent concentration modes.

The variance of the scalar concentration mode associated with frequency f^{II}, c^{II}, is presented in fig. 7(b). This was observed to persist throughout the whole streamwise extent of the domain and remained remarkably "coherent" throughout the space occupied by both the coherent velocity modes u^{III} (fig. 7(c) and u^{II} (fig. 7(a)), i.e those associated with both the small and medium wakes. Concentration mode c^{III}, associated with frequency f^{III}, is presented in fig. 7(d) and displays the partitioning between the "inner" and "outer" shear layers of the wake of the small bar but does not persist far beyond the wake intersection point. This multi-scale triple decomposition thus supports the finding that the primary coherent motion associated to the larger of the two (asymmetric) interacting wakes is the primary driver of the SSU mechanism.

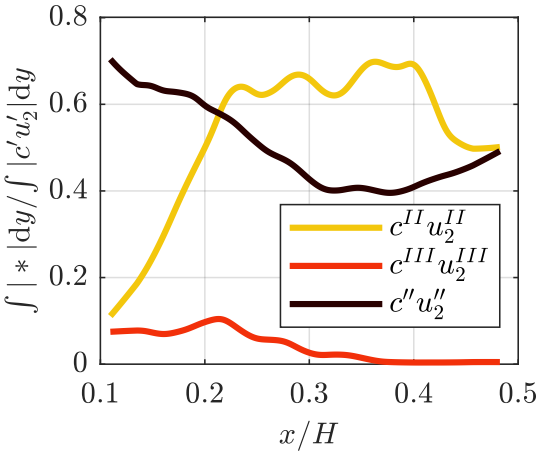

Figure 8: Ratio between transverse integrals of particular scalar flux components and the total scalar flux.

Figure 8 shows the scalar flux, decomposed into contributions from the various coherent fluctuations and the residual/stochastic fluctuation. Only the fluxes $c^{II}u^{II}$ and $c^{III}u^{III}$ were non-negligible from the coherent fluctuations but it can be seen that downstream of the wake intersection point the flux associated with the larger of the two interacting fundamental coherent motions ($c^{II}u^{II}$) dominates. It exceeds the scalar flux from the stochastic fluctuations after the wake intersection point and can be linked to the scalar bursting phenomenon identified in fig. 5.

Figure 5 clearly shows a spatially repeating pattern of scalar bursts in which there are large transverse excursions of the scalar from the small wake to the medium wake. These bursts appear, at least, to originate close to the wake intersection point between the small and medium wakes. We shall now consider conditional averages of both the scalar and velocity fields based upon the appearance of these scalar bursts.

Briefly, transverse profiles of the instantaneous concentration field are "stitched" together into a single spatio-

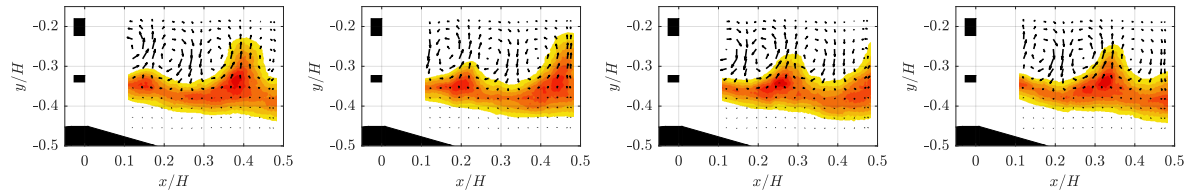

Figure 9: Conditionally averaged concentration fields (arbitrary scale), normalised with local maxima, overlayed on the associated conditionally averaged velocity field evaluated for phase values $\hat{\phi} =$ (a) 0, (b) $\pi/2$, (c) π and (d) $3\pi/2$.

temporal representation of the flow (i.e. as if Taylor's hypothesis has been applied). The locations of the maximum and minimum excursion (in the transverse direction) of a particular iso-contour of scalar concentration are then obtained. The maxima are assigned a phase value of 0 and the minima are assigned a phase value of π whilst the space between adjacent maxima (or minima) is linearly interpolated into 64 phase bins such that each snapshot could be assigned to a particular phase bin. The snapshots were then phase averaged according to this phase partitioning. A full description of this methodology is presented in Baj & Buxton (2019).

Figure 9 shows the phase evolution of these resolved conditionally averaged velocity and concentration fields. It can be seen that transverse scalar bursts appear to be driven by vortical structures shed from the medium bar (the larger of the two interacting wakes). A positive velocity is induced between two consecutive vortices when the upstream vortex rotates in an anti-clockwise sense and the subsequent vortex rotates in a clockwise sense. This induced gust transports the dye from the smallest wake into the medium wake. Further, the vortical structures modify the distribution of the scalar inside the small wake by transporting it towards the induced gusts. It is hard to distinguish precisely where the bursts begin to form simply from these conditional averages. When the conditionally averaged burst arrives at the wakes' intersection point, visible in fig. 9(b), it certainly already exists. Arguably, it already exists in fig. 9(a).

CONCLUSIONS

Combined PIV and PLIF experiments were conducted in the near-wake region of a multi-scale array of bars. Distinct secondary peaks were observed in the PSDs of the transverse velocity fluctuations at, and downstream of, the intersection point between two adjacent interacting wakes. These appeared at frequencies $f^a \pm f^b$, where f^a and f^b are the frequencies affiliated with the primary shedding mechanism of the two wake-generating bars. A multi-scale triple decomposition was performed on the velocity field and thus a multi-scale triple decomposed energy budget was derived for the coherent velocity fluctuations. This yielded new terms describing the transfer of energy between triads of coherent velocity fluctuations, which combined were termed the triadic production term. This term was shown to be responsible for providing the energy for the secondary coherent velocity modes.

Scalar was then introduced into the wake of the smallest bar in order to mimic the SSU mechanism as postulated by Laizet & Vassilicos (2012). Repeating bursts were observed in which scalar was rapidly transported from the small wake to the medium wake, thereby verifying the concept of the SSU mechanism. It is shown that the coherent velocity fluctuations (as opposed to the overall or stochastic velocity fluctuations) are the most influential in driving the SSU mechanism. The spectral results clearly show us that the primary (shedding) coherent mode associated with the larger of the two interacting wakes is the primary driver of these scalar bursts, providing the biggest contribution to the overall scalar flux downstream of the wake intersection point. This is reinforced by the conditionally averaged picture which shows that adjacent vortical structures within the larger of the two interacting wakes are responsible for forming these scalar bursts. There is only negligible contribution to the scalar transport from either the primary coherent structures in the smaller wake or the secondary coherent structures observed in the PSD of the velocity fluctuations.

REFERENCES

Baj, P, Bruce, P J K & Buxton, O R H 2015 The triple decomposition of a fluctuating velocity field in a multiscale flow. *Physics of Fluids* **27** (7), 075104:1–24.

Baj, P, Bruce, P J K & Buxton, O R H 2016 On a PLIF quantification methodology in a nonlinear dye response regime. *Experiments in Fluids* **57** (6), 1–19.

Baj, P & Buxton, O R H 2017 Inter-scale energy transfer in the merger of wakes of a multiscale array of rectangular cylinders. *Physical Review Fluids* **2** (11), 114607.

Baj, P & Buxton, O R H 2019 Passive scalar dispersion in the near wake of a multi-scale array of rectangular cylinders. *Journal of Fluid Mechanics* **864**, 181–220.

Cafiero, G, Discetti, S & Astarita, T 2014 Heat transfer enhancement of impinging jets with fractal-generated turbulence. *International Journal of Heat and Mass Transfer* **75**, 173–183.

Goh, K H H, Geipel, P, Hampp, F & Lindstedt, R P 2013 Flames in fractal grid generated turbulence. *Fluid Dynamics Research* **45** (061403), 1–22.

Hussain, A K M F & Reynolds, W C 1970 The mechanics of an organized wave in turbulent shear flow. *Journal of Fluid Mechanics* **41** (02), 241–258.

Laizet, S & Vassilicos, J C 2012 Fractal space-scale unfolding mechanism for energy-efficient turbulent mixing. *Physical Review E* **86** (4), 46302.

Laizet, S & Vassilicos, J C 2015 Stirring and scalar transfer by grid-generated turbulence in the presence of a mean scalar gradient. *Journal of Fluid Mechanics* **764**, 52–75.

Wynn, A, Pearson, D S, Ganapathisubramani, B & Goulart, P J 2013 Optimal mode decomposition for unsteady flows. *Journal of Fluid Mechanics* **733**, 473–503.